Numerical Calculations for Problems of Ductile Fracture

ROBERT M. McMEEKING
Materials Department and Mechanical Engineering Department, College of Engineering, University of California, Santa Barbara, California 93106, USA

ABSTRACT

Numerical calculations for problems of ductile crack growth carried out by the author are reviewed. These problems involve crack tip blunting in thick and thin sheets, the growth of voids near blunting crack tips and the modelling of void-crack coalescence. The most recent calculations have been carried out in three-dimensions and substantial detail is revealed.

KEYWORDS

Ductile fracture; finite elements, crack blunting, void growth.

INTRODUCTION

When an elastic-plastic body with a sharp crack is subjected to a monotonically increasing load of mode I type (i.e., tensile opening), blunting of the tip by intense straining will occur until some mechanism of crack extension takes over. The stress and deformation fields near a blunt crack are quite different from those predicted by the analysis of a mathematically sharp crack. If finite geometry changes (i.e., blunting) are ignored, the stress and deformation fields near the tip of a tensile, mathematically sharp crack, in a power-law hardening material are governed by the one parameter singularity derived by Hutchinson (1968a) and Rice and Rosengren (1968) (HRR fields). The HRR field shows that the most extensive straining appears above and below the crack tip rather than directly ahead of it; large stresses are also predicted ahead of the crack. However, if crack tip blunting is taken into account, a completely different picture emerges. As was first shown by Rice and Johnson (1970), intense strains now appear directly ahead of the crack over a distance comparable in size to the crack tip opening displacement (COD); also, the stress boundary conditions on the

deformed crack surface limit the hydrostatic stress elevation ahead of the crack and result in lower stresses ahead of it.

The predominant ductile fracture mechanism is void nucleation, growth and coalescence. Since hole growth itself is a finite strain process and the size of the fracture process zone is comparable to the COD, it becomes clear that in relating the results of continuum analyses to microstructural fracture events one must take crack tip blunting into account.

Detailed finite element analyses (McMeeking, 1977a) show that the stresses and strains near a crack tip at loads less than the fracture load are well above those which would have caused failure in a macroscopically homogeneous deformation field. As discussed by Rice (1976), this suggests that in relating microstructure to the conditions for fracture initiation, it is important not only that some critical stress or strain be achieved ahead of the crack tip, but also that they be achieved over a microstructurally significant size scale for the fracture mechanism at hand. Rice (1976) also mentions that the need for a relation between macroscopic toughness and microstructure is clear from dimensional considerations alone, in that the critical fracture toughness (K_{Ic}) or the critical crack tip opening displacement (b_f) must depend not only on material parameters which enter the constitutive law, like the yield stress and the elastic moduli, and critical stress and strain values, but also on some characteristic length of the material, such as grain size or inclusion size and spacing.

In the following, we first discuss crack tip blunting in some detail; then, we present results for the near crack type growth of voids nucleated at inclusions and examine the effects of inclusion size and spacing on the conditions for fracture initiation. This work includes some recently solved three-dimensional problems.

CRACK TIP BLUNTING ANALYSIS

Rigid-Plastic Analysis

Rice and Johnson (1970) were the first to study crack tip blunting in detail. They suggested that the blunting can take place by a general stretching of material on the crack tip. Near tip rigid-plastic slip line solutions were taken as good approximations to the behavior of elastic–plastic materials, when elastic strains are neglected compared to plastic strains. They considered the cases of the contained yielding of a plane strain, non-hardening specimen (CY specimen), and the fully plastic yielding of a deeply cracked, double edge-notched, thick panel of non-hardening material (DEN panel). One approach to both of these problems is to view the crack tip as a point of singular shear strain, and the slip line field of Fig. 1 arises in this case. In the DEN panel, Fig. 1 is the near tip region of the Prandtl punch type plastic zone that arises for full scale yielding; the CY specimen has this slip line field only in a near tip region that is small compared to the plastic zone as discussed by Rice (1968). A straight slip line in

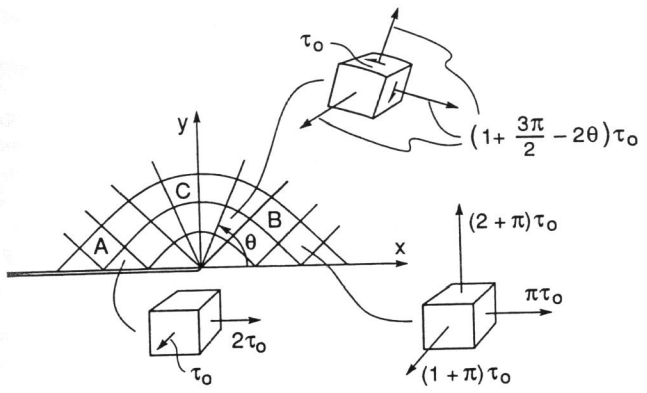

Fig. 1. Near tip stresses and slip line field

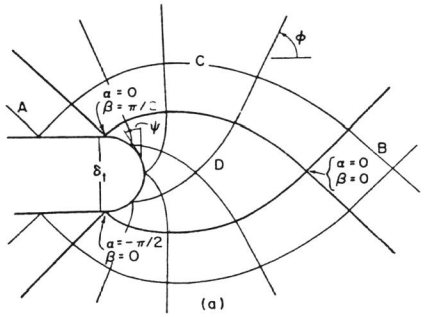

Fig. 2. Slip line field around smoothly blunted crack tip

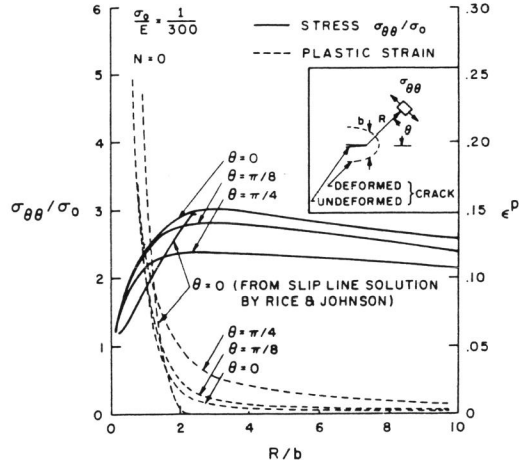

Fig. 3. Plot of stress and plastic strain around the blunted crack

AFR-3—D

region C transmits a constant velocity parallel to itself and this velocity was calculated for both the CY specimen and the DEN panel.

Rice and Johnson (1970) noted that when the crack blunts, the fans of singular shearing above and below the crack tip would become noncentered above and below a region of intense stretching adjacent to the blunted crack tip as in Fig. 2. When viewed on the size scale of the plastic zone, this whole region of intense stretching still appears as a point, so the velocities in region C of Fig. 1 still serve as approximations to the normal velocities on the outer slip lines of the intensely stretched zone. They used these velocities as boundary conditions to solve the slip line equations numerically for the velocities at D as functions of α and β. They also showed that the position of the crack tip relative to the point $\alpha = 0, \beta = 0$, can be worked out once the velocities on the crack tip are known. Once the physical coordinates of the points on the blunt crack tip are known, the physical coordinates throughout region D can be determined numerically.

Their results show that large strains appear directly ahead of a crack tip when finite geometry changes are considered, but only in a region adjacent to the blunting tip. This means that in situations for which large strains are required for fracture (e.g., ductile growth of microvoids nucleated at inclusions), the COD at fracture (b_f) must be such that the large strain region D envelops characteristic microstructural dimensions in the separation process. Their results also show that with consideration of actual geometry changes at the crack tip, the maximum stress achievable over any reasonable size scale of the material is limited, contrary to the predictions of the HRR field. They also showed that the shape of the blunt crack tip is given by

$$\underset{\sim}{r}(\psi, \delta_t) = \underset{\sim}{r}(\psi, 0) + \underset{\sim}{f}(\psi)\delta_t \tag{1}$$

where $\underset{\sim}{r}$ is the position vector of points on the tip, ψ and δ_t are the tangent angle and the notch opening, respectively (Fig. 2), $\underset{\sim}{f}$ is a vector valued function of ψ, and $\underset{\sim}{r}(\psi, 0)$ is the position vector before deformation. For an initially sharp crack $\underset{\sim}{r}(\psi, 0) = 0$, and

$$\underset{\sim}{r}(\psi, \delta_t) = \underset{\sim}{f}(\psi)\delta_t \tag{2}$$

Equations (1) and (2) show that the shape of the tip of a notch can be obtained at all times by adding the original notch shape to the steady-state shape of a sharp crack blunted by the same loads. Thus, as the total notch opening grows several times the original notch opening, the difference between the blunted notch shape and the shape of the sharp crack blunted by the same loads become negligible. Under small-scale yielding conditions, the steady-state shape of the

blunted sharp crack arises because the COD is the only length of significance in the near tip region and displacements and all other distances scale with it.

Elastic-Plastic Analysis

Based on the above results, McMeeking (1977a) used large deformation finite elementary analysis to model the blunting of a sharp crack under small-scale yielding plane strain conditions, even though the tip actually had a finite root-radius in the undeformed configuration. He considered both non-hardening and hardening elastic–plastic materials. The constitutive law he used represents the J_2 flow theory and accounts for rotation of the principal deformation directions. The finite element formulation was based on the updated Lagrangian method of McMeeking and Rice (1975) for large deformation of elastic–plastic materials, modified according to Nagtegaal, Parks and Rice (1974) to free the mesh of artificial constraints on the incompressible modes. The small-scale yielding solution is achieved by applying displacement boundary conditions remote from the crack tip to impose an asymptotic dependence on the mode I elastic crack tip singular stress field. More details are given McMeeking (1977a) and will not be repeated here.

Figure 3 shows the true stress $\sigma_{\theta\theta}$ (see inset of Fig. 3) normalized by the true tensile yield stress σ_o, vs. the distance from the notch tip in the undeformed configuration for an elastic perfectly-plastic material. The distance is normalized by the current notch opening, which allows results from the later increments of the finite element calculations to be plotted together. As the notch tip is approached at a given angle to the crack line in the undeformed configuration, the stress rises due to increasing strain. However, the hydrostatic stress cannot be maintained on the blunted notch surface and as a result, there is a maximum for $\sigma_{\theta\theta}$, coinciding with a maximum for hydrostatic stress, some distance from the notch tip. Figure 3 also shows equivalent plastic strain plots from the later increments of the finite element solutions. The strains are clearly small except very close to the blunted tip. Outside the near-tip region, the larger plastic strains are on the lines at an angle to the crack line and this is in agreement with the HRR results. However, close to the tip, the situation is reversed and the plastic strains are larger than 5.

For comparison, the stress and plastic strains ahead of the crack ($\theta = 0$) from the slip line solution of Rice and Johnson (1970) have been plotted in Fig. 3. The agreement between the finite element results and the slip line results are quite close as far as the position and magnitude of the stress maximum are concerned.

Similar finite element calculations for power-law hardening materials show that the magnitude of the stress at the maximum is higher and that the position of the stress maxima move closer to the notch tip. Another hardening effect is an upturn in stress close to the notch surface, which arises from the elevation of flow stress by the large plastic strains in this area. In fact, when a sharp crack in a power-law hardening material is blunted to a finite width, infinitely large stress

on the notch surface will arise, but only over a distance small compared to the blunted-crack width. This stress singularity arises because in the power-law hardening model, infinite plastic strains produce infinite flow stresses, whereas a saturation to a constant flow stress after large plastic strains is more physically realistic. In addition, few cracks are likely to be atomistically sharp and the finite radius at the tip of most real cracks will lead to only large but finite plastic strains at the tip.

Additional results for the near tip stress and deformation fields as well as for the shape of a blunting crack tip were obtained by Tvergaard and Needleman (1983).

Blunting of a Crack Tip Into a Shape with Corners

In the last two sections, smoothly blunted crack tips were considered. However, the shape of the blunted tip is not unique, at least within the rigid-plastic model for non-hardening materials. The blunted tip shape may have two or more sharp corners, or be smoothly curved. McClintock (1971) has given slip line fields that arise around crack tips that are blunt by localized shearing at corners on the crack tip. The corners on the crack tip are connected by straight segments of crack tip surface and McClintock has worked out slip line fields with two and with three corners on the crack tip. McClintock (1971) has observed also the opening of a macroscopic notch by a mechanism of shearing at two corners, while Clayton and Knott (1976) have observed localized shearing at many corners on a macroscopic notch tip. Rawal and Gurland (1976) have observed the smooth mechanism of blunting in the opening of prefatigued crack in spheroidized steel. The type of blunting which arises in a specific case may depend on considerations of strain hardening and stability. The tendency for deformation to localize at, say, asperities on the tip surface may be important in this respect. Apart from the shape, the main difference between the smoothly blunted crack tip case and the case with the sharp corners is that the sharp corners are the focus of fans with singular shear strain rates. It is these that largely accommodate the crack tip opening by transporting material from the interior to create new surface.

McMeeking (1977b) studied in detail the blunting of a crack tip into a shape with corners using the method of slip lines which were found numerically. The crack tip shapes and slip lines for the case of blunting with two corners on the tip and with three corners on the tip are shown in Figs. 4 and 5. McMeeking's (1977b) results show that the stretches on the x-axis remain relatively small compared to the larger values near the tip of a smoothly blunted crack. However, at distances farther than one notch opening from the tip, a slightly more severe strain state is achieved in the cases where the crack has blunted by the sharp corner mechanism. In terms of a fracture process that occurs when a critical strain is achieved over a critical length, the COD at fracture would be slightly greater in the smoothly blunted case compared to the sharp-nosed case; that is, if the x-axis strain is typical. The sharp-nosed case would show a slightly larger COD at fracture compared to the flat-nosed case, at least based on crack growth occurring on the x-axis.

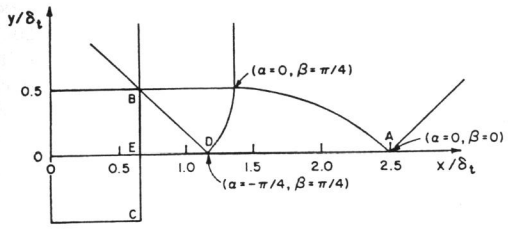

Fig. 4. Blunting of a crack into a shape with two vertices

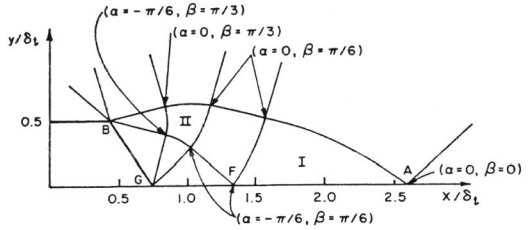

Fig. 5. Blunting of a crack into a shape with three vertices

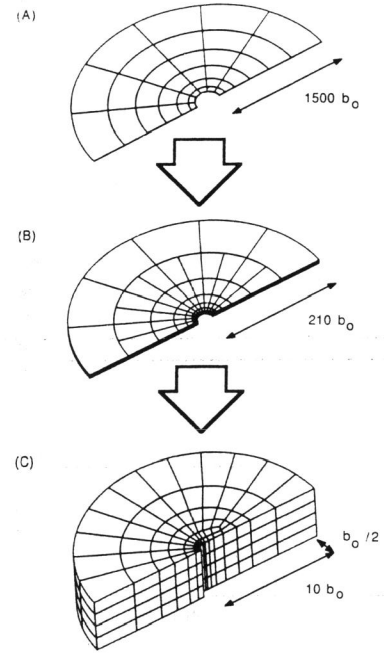

Fig. 6. The three-dimensional finite element mesh used to solve the boundary value problem.

Following Rice and Johnson (1970), McMeeking (1977b) also obtained an approximation for the near tip stresses for power-law hardening materials. His results show that the stresses for blunting with corners on the crack tip in the CY specimen would be slightly smaller than those in the smoothly blunted crack. In terms of a fracture event controlled by a critical stress that must apply over a critical distance, specimens with smoothly blunted crack tips would appear to be marginally less tough than those which have cracks blunted by the sharp corner mechanism.

Detailed finite element analyses of the near tip stress and deformation fields were also carried out by Needleman and Tvergaard (1983). Following McMeeking and Parks (1979), they focused on the question of when the blunted crack tip region is uniquely characterized by a single parameter such as Rice's (1968) J-integral, or equivalently, on the minimum specimen size requirements for valid J-tests. They carried out calculations for deeply cracked center-cracked panel (CCP) and single-edge crack bend (ECB) specimens. They based their calculations on the phenomenological corner theory of plasticity, termed J_2 corner theory, proposed by Christoffersen and Hutchinson (1979). One immediate consequence of the presence of a vertex on the yield surface is that yield surface vertex effects permit shear band development at achievable strain levels in strain-hardening solids, whereas the classical smooth yield surface elastic-plastic work hardening solid is quite resistant to the localization of deformation in a shear band. Their results show that the highly localized deformation accompanying shear banding leads also to near tip strain fields very different from that predicted by the classical smooth yield surface model. The initially smooth notch tip of the ECB specimen was flattened out and shear bands developed from the corners of this flattened region. Similar results were found for the early deformation stages of the CCP specimen. As mentioned by Needleman and Tvergaard (1983), the flattening out of a curved surface at the initiation of shear band development has been encountered in previous calculations and is associated with the attainment of a critical strain for a short-wavelength surface instability at the free surface.

Blunting in Thin Sheets

The results discussed so far are for plane strain problems. As long as the thickness of the material is much greater than the bluntness of the crack, the plane strain model is satisfactory. Thus, even in a thin sheet, the situation at the crack tip will be plane strain if the COD is small compared to the plate thickness. In such circumstances, elastic thinning of the sheet or the development of a plastic zone having a plane stress character could dominate the behavior of the near tip region in the thin plate. These features have been considered in such papers as Narasimhan and Rosakis (1988) and Nakamura and Parks (1987). However, in circumstances where the sheet is extremely thin or the notch is very blunt, the width of the notch can be comparable to the thickness of the sheet. In those circumstances, the blunting deformations take place within a plane stress-like environment. To provide insight into this situation, Hom and McMeeking (1988a) carried out three-dimensional calculations of blunting of a crack in a thin sheet. Prior work on this particular

issue is confined to research by Nishimura and Achenbach (1986) in plane stress who matched an approximate solution for the deformation gradient directly ahead of the blunt tip to an outer solution due to Thomason (1979) which is similar to the HRR field.

Hom and McMeeking (1988a) considered mode I loading in small-scale yielding and plane stress far away from the crack tip was imposed. However, a near tip enclave was treated in a fully three-dimensional fashion. This tip region was sufficiently large so that all the three-dimensional effects occurred there and only there. An asymptotic dependence on the mode I elastic crack tip singular plane stress field of Irwin (1960) was obtained by incrementally applying displacement boundary conditions remote from the crack tip. The constitutive law for the material used was J_2 flow theory (Von Mises criterion with an associated flow law) with an adjustment to the elasticity for the rotation of the principal deformation axes. This form of the constitutive law is discussed by McMeeking and Rice (1975). Both perfectly plastic and power-law strain hardening results were obtained, but only the non-hardening solution will be considered here. The uniaxial yield strain was 0.01 and Poisson's ratio was 0.3.

The sheet had an initial thickness of t_0 and the crack had an initial notch width of b_0. The ratio t_0/b_0 is the only length ratio of significance to the problem, and it was chosen so that the plastic zone could become large eventually compared with the sheet thickness. The three-dimensional zone near the crack tip was eventually surrounded by yielded material and a stress field conforming to Hutchinson's (1968b) plane stress solution developed there outside the region where the three-dimensional effects were important. Ratios of 5 and 10 for t_0/b_0 were used. The coordinate system used was chosen so that the sheet's out-of-plane dimension is the Z-axis. The origin was chosen so that the midplane of the plate is $Z = 0$ and $Z = t_0/2$ was one of the plate's free edges, the other being at $-t_0/2$. The X-axis lies at the intersection of the crack plane and the midplane of the sheet.

The finite element method was used to solve the boundary value problem formulated in the previous section. The general finite element program ABAQUS (1984) was used to perform the computations. The three-dimensional finite element mesh used to solve the problem of a crack in a thin sheet is shown in Fig. 6(a,b,c). Due to the symmetry of the loading, only one fourth of the sheet was modelled. That is, the mesh represents the portion of the specimen for which $Z \geq 0$ and $Y \geq 0$ and boundary conditions were used to impose symmetry conditions on the planes $Z = 0$ and $Y = 0$. The mesh in Fig. 6(a) is one element deep and surrounds the mesh in Fig. 6(b). The mesh in Fig. 6(b) is two elements deep and surrounds the mesh in Fig. 6(c). Finally the mesh in Fig. 6(c) contains the crack tip and is four elements deep. The outer semicircular perimeter of the mesh is 3000 times the initial radius of the crack's tip. There were a total of 3344 nodes and 440 twenty noded brick elements in the mesh.

Deformed Crack Tip Configurations The deformed crack tip shapes with $t_o/b_o = 5$ for the sheet's midplane ($Z = 0$), quarter plane ($Z = t_o/4$) and free surface ($Z = t_o/2$) are shown in Fig. 7 for the non-hardening ($N = 0$) case at load level $J/\sigma_o b_o = 2.0$ where J is the J-integral of Rice (1966) (Note that Z is the position on the Z-axis of material points in the undeformed state). The dashed lines denote the undeformed mesh while the solid lines indicate the deformed mesh. The COD is independent of Z and is currently about $3b_o$. This amount of blunting is sufficient to give characteristic results independent of the fact that the original notch width was finite. All results discussed are for this load level. Figure 7 indicates that the deformation near the tip of the crack is three-dimensional in nature. In the midplane of the sheet the deformation is concentrated directly ahead of the crack tip, and elements at the crack tip along the plane of symmetry are stretched by large amounts in the tensile direction. The deformation at the free edge and the quarter plane is more evenly distributed about the crack tip. The deformed meshes for a perfectly plastic material and a strain hardening one are generally similar. However the tip elements in the hardening case are slightly less distorted at the midplane due to the strain inhibiting effect of the hardening.

Figure 8 shows a plan view of the deformed crack plane for the non-hardening case for $t_o/b_o = 5$. The results show that the crack advances due to blunting more rapidly at the midplane of the sheet than at the free surface, and the shape of the crack front creates a lip at the edge of the plate. The figure also indicates that large out-of-plane displacements make the sheet very thin in the region near the crack tip. The finite element results show also that there is a linear relationship between the crack tip opening displacement and the J-integral as expected from previous work. For an initially sharp crack, the coefficient n for the relationship $b = nJ/\sigma_o$ is essentially unity for the non-hardening case and is less for the strain-hardening material. The former result agrees very well with the linear plastic zone model of Dugdale (1960) for plane stress whereas the crack opening is much less in plane strain (McMeeking, 1977a). The finite element case with the smaller sheet thickness agrees very well with the Dugdale result. For the larger sheet thickness, the finite element result for crack opening at the midplane is less and is a little closer to the behavior of a plane strain crack. With increasing sheet thickness, the crack tip opening displacement at the midplane should approach the plane strain behavior. However, a simple extrapolation of the finite element results shows that the thickness must approach $t_o/b_o = 80$ for plane-strain-like behavior to occur at the midplane.

Stress and Strain Distributions In The Near Tip Field In Fig. 9, the near tip stress $\sigma_{\theta\theta}$ directly ahead of the crack at Θ is plotted versus distance to the crack for the case $t_o/b_o = 5$ and $N = 0$. Directly ahead of the crack tip, the stresses at the midplane are higher than the stresses at the free edge. This reflects a somewhat high triaxiality of the near tip stress field at the midplane Since the hydrostatic stress along the edge of the sheet is constrained by the free surface, $\sigma_{\theta\theta}$ is lower there and roughly uniform. At the midplane, $\sigma_{\theta\theta}$ is higher since there is no

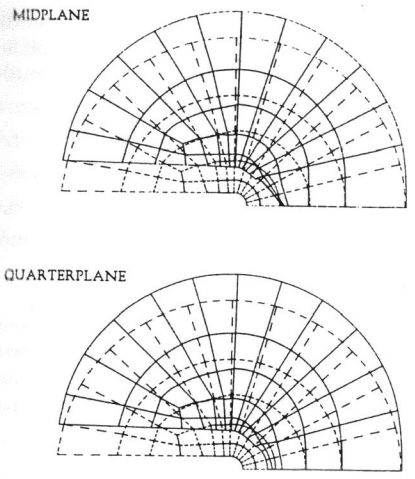

Fig. 7. The deformed mesh at the sheet's midplane, quarter plane and free surface for $N = 0$ and $t_o/b_o = 5$ at a load level $J/\sigma_o b_o = 2.0$. Dashed lines indicate the undeformed mesh.

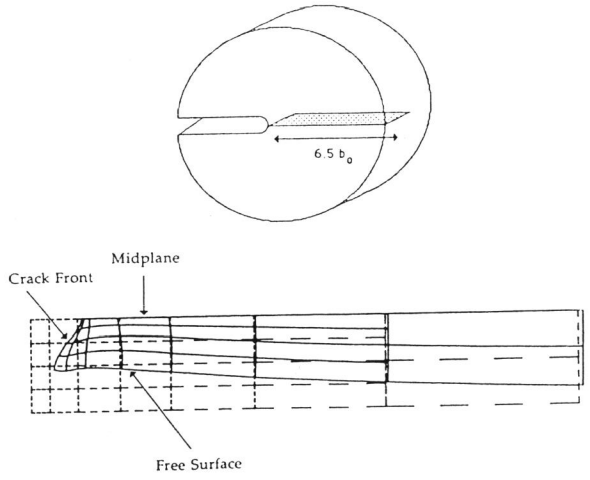

Fig. 8. The deformed mesh in the crack plane for $N = 0$ and $t_o/b_o = 5$ at a load level $J/\sigma_o b_o = 2.0$ superimposed on the undeformed mesh.

free surface to impose a constraint on the hydrostatic stress and triaxiality builds up in the standard fashion. However, the hydrostatic stress along the midplane cannot be maintained on the surface of the crack tip, and therefore a maximum in $\sigma_{\theta\theta}$ exists corresponding to the maximum for hydrostatic stress, some distance from the notch tip. The stress maximum occurs directly ahead of the crack ($\theta = 0$) and its value is approximately $2\sigma_0$. At angles of 30^o and 60^o to the crack tip, the stresses in the near tip region are highest at the free edge of the plate and indeed $\sigma_{\theta\theta}$ is mostly compressive at these angles (See Hom and McMeeking, 1988a).

Figure 9 indicates also the extent of the three-dimensional stress state near the crack tip. Adjacent to the tip, the stresses depend on the position of the material point through the thickness. However, further afield from the crack tip, the stresses become independent of that coordinate. Thus plane stress conditions prevail there. At $\theta = 0$, the three-dimensional region extends out to about $6t_0$, whereas at $\theta = 30^o$ it spreads only as far as $3t_0$. This is much greater than previous estimates of this region. At the stage represented by Fig. 9, the crack tip opening is about 60 percent of the original thickness. At larger relative openings one would expect there to be a different extent of the three-dimensional stress region.

The solutions of Hutchinson (1968b) for a sharp plane stress crack tip and Nishimura and Achenbach (1986) for a blunting plane stress crack tip are also plotted in Fig. 9. As expected, the plane stress solutions agree with the finite element results ahead of the crack at the free surface of the sheet and underestimate the stresses at the midplane. The stresses at all three sections approach the plane stress solution far away from the crack tip. On the other hand, the stresses at the midplane near the crack tip are not as high as the maximum stresses predicted by Rice and Johnson (1970) and McMeeking (1977a). In that case, $\sigma_{\theta\theta}$ reaches a maximum value of $3\sigma_0$, and therefore a plane strain field does not develop even at the midplane near the crack tip in the thin section results.

Ahead of the crack, the strain concentrates into two relatively narrow crossed bands. This feature is seen most clearly in the contour plot of the effective plastic strain shown in Fig. 10 for a cross section of the sheet at a distance of 4.25 b_0 ahead of the crack tip. Most of the plastic strain is concentrated at the crack tip in the midplane of the sheet. Two shear bands similar to the cross slip observed by Dugdale exist directly ahead of the crack tip on planes approximately 45^o to the plane of the sheet. This double shear band accounts for the large deformation seen at the midplane directly ahead of the crack tip and at the free edge for $\theta = 30^o$ and 60^o. However, these shear bands are contained well inside the plastic zone which extends to about 40 times the original sheet thickness at this stage of loading (see Fig. 11). Thus, the double shear band region does not represent the plastic zone by itself as was assumed by Dugdale (1960). Instead, there is a region of diffuse yielding around the shear bands. Figure 10 does show

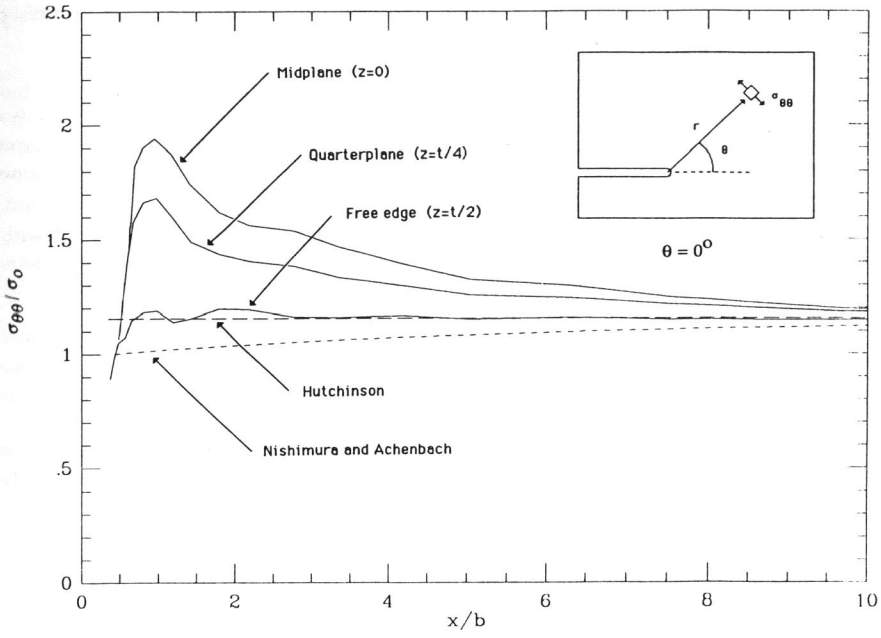

Fig. 9. The near tip stress fields for the case $N = 0$, $t_0/b_0 = 5$ and $\theta = 0^o$ at a load level $J/\sigma_0 b_0 = 2.0$.

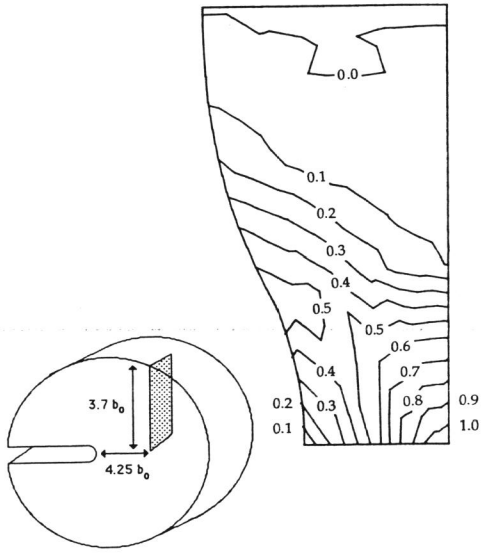

Fig. 10. A contour plot of effective plastic strain for a cross section ahead of the crack tip for the case $N = 0$, $t_0/b_0 = 5$ at a load level $J/\sigma_0 b_0 = 2.0$.

clearly, however, that there is a significant amount of localized thinning associated with the high plastic strains near the crack tip.

Plastic Zone Shapes Except in the early stages of straining, the thickness of the plate was small compared with the plastic zone and the solution away from the crack tip was like plane stress. Therefore, the plastic zone is of uniform shape through the thickness of the sheet. However, Fig. 11 shows that the plastic zone is not self similar at different load levels $J/\sigma_0 b_0$ for the non-hardening material. The plastic zone does not spread transverse to the crack but extends ahead with increasing load. For the non-hardening case, the finite element results relate the length of the plastic zone on the x-axis r_p to the J-integral by $r_p = 0.28EJ/\sigma_0^2 = 0.28(K/\sigma_0)^2$ where K is the stress intensity factor. These plastic zone sizes from the finite element calculation are smaller than those predicted by the small strain technical plane stress theories. The coefficient is 0.393 according to the model of Dugdale (1960) and 0.300 from the analysis of Achenbach and Dunayevsky (1984). The shape of the plastic zone seems to be influenced by the crossed shear band mechanism ahead of the tip. This seems to limit the spread of the plastic zone in the transverse direction and so concentrate it ahead of the crack.

Comparison with Experimental Results A comparison can be made between the finite element results of Hom and McMeeking (1988a) for the case $N = 0.1$ and $t_0/b_0 = 10$ (which are quite similar to the perfectly plastic case) and the displacement field measured by Wu and Chiang (1986) for thin sheets of Al 6061-T6 using a combined laser speckle-moiré method. The material and geometric parameters for the experiment were $N = 0.054$, $E/\sigma_0 = 246.$ and $t_0/b_0 = 8$. Thus, there is some discrepancy between the parameters involved in the experiments and the calculations. Figure 12 shows the out-of-plane displacement directly ahead of the crack tip obtained by Wu and Chiang, as well as that arising in the finite element calculation. Generally the agreement is good between the two results. However, the finite element computation predicts slightly lower displacements ahead of the crack than observed experimentally. One reason for this difference is that the specimen used in the experiment was thinner and made of a lower hardening material than the specimen modelled in the finite element calculation. Thin sheets made of non-hardening materials deform out of plane more than thicker sheets of hardening material (Hom and McMeeking, 1988a). The displacements at 30° to the crack plane predicted by the finite element analysis are closer to the experimental results. Therefore the finite element solution's out-of-plane displacements are more diffuse and less concentrated than the displacement field observed experimentally.

DUCTILE VOID GROWTH NEAR A CRACK TIP

In ductile metals, failure by coalescence of microscopic voids is an important fracture mechanism both in nominally uniform stress fields and ahead of an

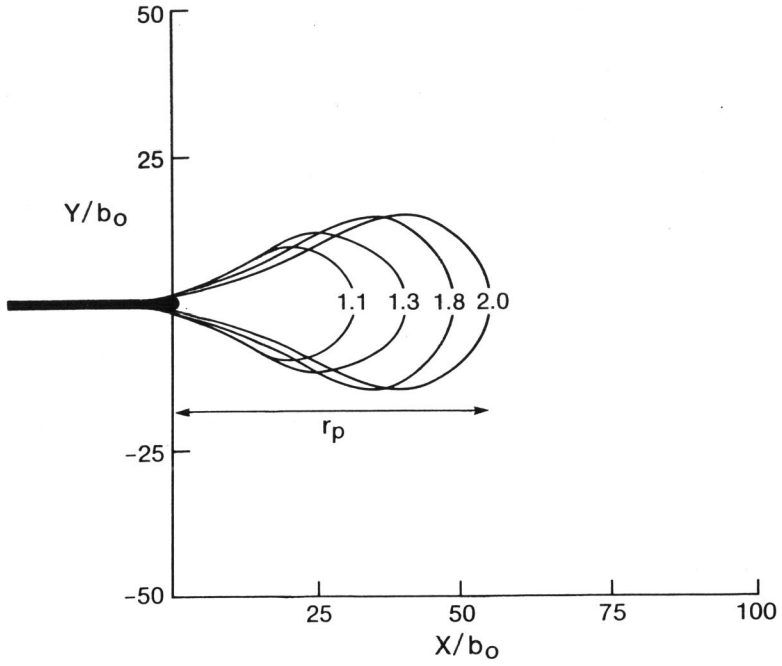

Fig.11. Plastic zones for $N = 0$ at various load levels, $J/\sigma_0 b_0$.

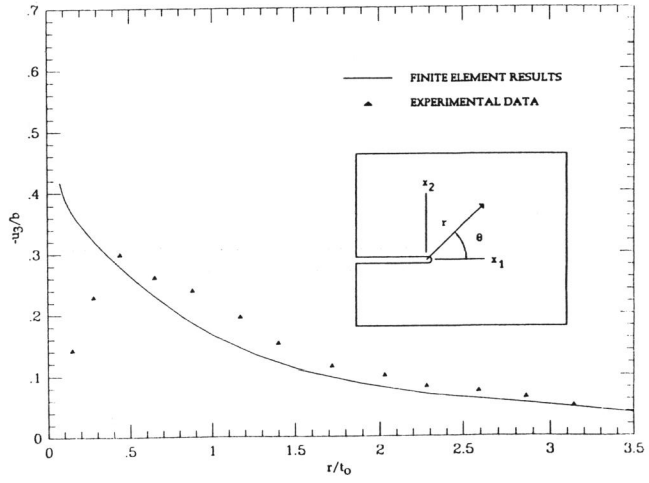

Fig.12. Comparison of the out of plane displacements predicted by the finite element analysis and measured experimentally by Wu and Chiang at $\theta = 0^o$.

existing crack. A mechanism has been proposed and confirmed by Low and his coworkers (Cox and Low, 1974, Van Stone, Merchant and Low, 1974) which is as follows: often two families of microvoids play an important role in the fracture process; the larger microvoids, which nucleate at relatively low strains, and the smaller-scale voids, which nucleate at considerably larger strains. The larger voids nucleate by fracture or interfacial decohesion of inclusions and grow due to plastic straining of the surrounding matrix material; fracture occurs when they are linked with each other or with the crack tip. The growth of the larger microvoids can be interrupted by the formation of void sheets between larger voids or between larger voids and the crack tip. These void sheets are composed of smaller microvoids nucleated at carbides or precipitate particles and lead to local failure. Experiments have been inconclusive as to whether voids formed on precipitates cause shear band localization or merely appear as a result of it. Although void nucleation is the subject of a great deal of research, the results are not yet so clear that conditions for nucleations can be used in void growth calculations. A critical normal stress at the matrix-particle interface (Argon and Im, 1975) or a critical strain of the matrix material (Brown and Embury, 1973) have been proposed as void nucleation criteria.

On the other hand, void growth has been studied by several researchers. The growth of a spherical void ahead of a blunting crack was analyzed in an approximate way by Rice and Johnson (1970), who used the results of Rice and Tracey (1969) for growth of a isolated cavity in a remotely uniform deformation field in a rigid-plastic material. Rice and Johnson (1970) identified the remote field of Rice and Tracey's (1969) analysis with their slip line solution (Fig. 2) for the local stress and deformation fields of a blunting crack computed as if no void were present. The strong interactions between the free surfaces of the void and the blunting tip were neglected, except for an approximation adopted to describe final coalescence of the void with the crack. The void was assumed to start growing once it was enveloped by the large-strain region ahead of the crack (region D in Fig. 2). Rice and Johnson (1970) assumed that the void grows until the distance between the void boundary and the blunted crack tip becomes equal to the vertical radius of the void. Then, it was assumed that final fracture occurs by localized necking of the remaining ligament, requiring an additional opening displacement to fracture equal to the ligament size. They also identified the initial distance of the void from the crack tip, D, with the average spacing between inclusions which nucleate voids, and the initial void radius with the average void nucleating inclusion size. In this way, they obtained estimates for the COD at fracture initiation, b_f, as a function of inclusion size and spacing. In similar work, McMeeking (1977a) studied the growth of spherical voids ahead of the crack tip and at 45° to it using his results from detailed finite element analyses of a blunting crack for both elastic perfectly-plastic and hardening materials. McMeeking's (1977a) results are in agreement with those of Rice and Johnson (1970) and the estimates for b_f/D are insensitive to the value of the hardening exponent and the orientation of the void to the crack plane. The results of Rice and Johnson (1970), McMeeking (1977a) and some more recent finite element results are discussed in more detail later on in this section.

Andersson (1977) studied the growth of a spherical void in a rigid-plastic cylindrical cell and presented a simplified model for the growth of spherical voids near a crack tip. Chiang (1981) used a finite element method to study the near crack tip hole growth and modelled the ligament between the hole and the crack tip with a compact tension specimen. Aoki et al. (1984) studied the crack tip blunting using Gurson's (1977a, 1977b) constitutive equations to describe the material behavior. They also studied the near crack tip hole growth and used the Rudnicki and Rice (1975) condition for localization of plastic flow in the ligament between the hole and the crack tip.

Cylindrical Holes Parallel to the Crack Tip

Aravas and McMeeking (1985a, 1985b) used large deformation finite element analysis to study the near crack tip growth of long cylindrical voids aligned parallel to a mode I plane strain blunt crack under small-scale yielding conditions. The results of the calculations provide a reasonable model for the behavior of holes generated by long stringers parallel to the crack, like those in specimens cut in the long transverse direction. Two different configurations were analyzed: one with a single hole ahead of the crack and one with two holes at 30° to the crack line. Several values of the spacing to size ratio of the inclusions were considered and the effects of this ratio on the conditions for fracture initiation were examined. In a first set of calculations (Aravas and McMeeking, 1985a), the elastic-plastic material was assumed to be fully dense and the presence of the smaller-scale voids in the ligament between the large void and the crack tip was not taken into account. The J_2 flow theory, suitably modified to account for rotation of the principal deformation axes, was used to describe the constitutive behavior of the material. Figure 13 shows the deformed finite element mesh in the near tip region superposed on the undeformed one (dashed lines) for the case of the void ahead of the crack. The deformed configuration for the case of the two voids at 30° to the crack plane is shown in Fig. 14. In both cases, the holes are pulled toward the crack tip and change their shape to approximately elliptical with the major axis radial to the crack. This shows that the effect of the interaction of the neighboring free surfaces on the hole growth is stronger than the effect of the mainly tensile stress field ahead of the crack tip. The results of Aravas and McMeeking (1985a) show that the cylindrical holes ahead of the crack grow faster than those at 30° and this is rather different from what has so far been inferred for the growth of spherical voids by McMeeking (1977a). Aravas and McMeeking (1985a) used several geometric criteria to predict localization of flow in the ligament between the voids and the crack tip; when the criterion for coalescence was satisfied, the hole growth was interrupted and crack extension was assumed to occur. At this point, the values of the J-integral and the COD for fracture initiation were obtained.

In a separate set of calculations, Aravas and McMeeking (1985b) took the presence of the smaller-scale voids into account by using Gurson's (1977a, 1977b) equations modified by Tvergaard and Needleman (1984) to model the constitutive behavior of the matrix material. Using the modified Gurson equations and a method proposed by Tvergaard (1982) to model material failure,

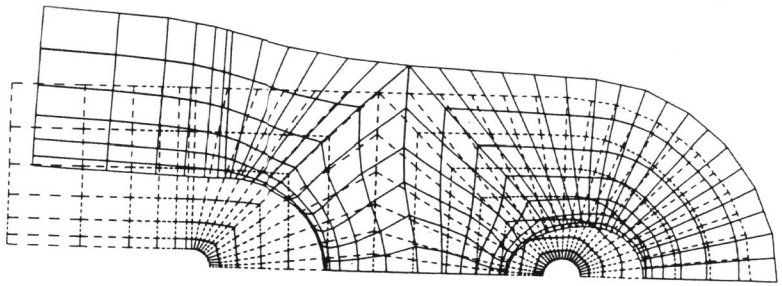

Fig. 13. Deformed finite element mesh in the near tip region superposed on the undeformed one (dashed line)

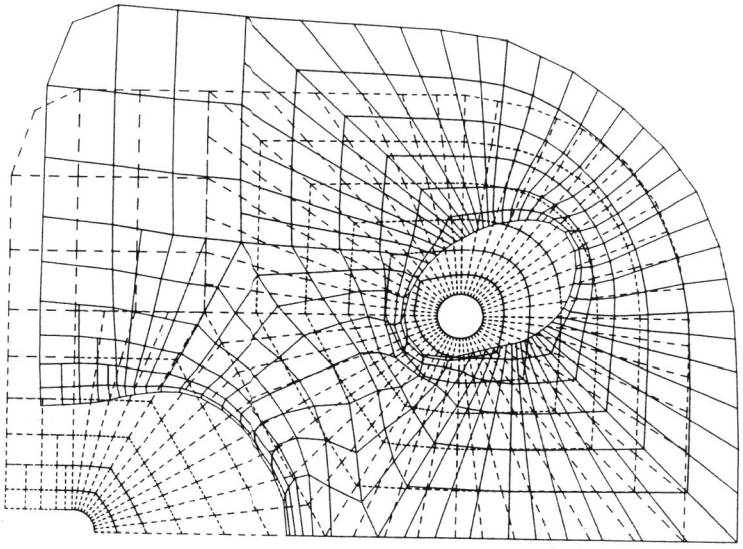

Fig. 14. Deformed finite element mesh in the near crack tip region superposed on the undeformed one (dashed line)

they also studied the formation and growth of the microcrack in the ligament between the larger hole and the crack tip. In this ways, the final stage of coalescence of the larger hole with the crack tip was analyzed in detail. The difference between the predicted values for the COD at fracture initiation between the Gurson and the fully dense material is small and this shows that the results obtained using the fully dense elastic-plastic material together with some geometric criterion to predict localization are, numerically, quite satisfactory.

Spherical Holes Near the Crack Tip

Hom and McMeeking (1988b) carried out large deformation finite element calculations for the growth of initially spherical holes directly ahead of a mode I plane strain blunting crack tip in an elastic-plastic material in small-scale yielding. Elastic-perfectly plastic and strain hardening calculations were carried out, but only the non-hardening results will be reviewed here. The yield strain in uniaxial tension was 1/300 and Poisson's ratio was 0.3. A periodic array of holes parallel to the crack was used so that the analysis could focus on a slice of material representing half the material between neighboring voids as shown in Fig. 15. Boundary conditions imposing the symmetry and periodicity were imposed on this cell to produce an overall plane strain response with respect to the crack tip. The crack and void surfaces were traction free. Around the perimeter of the outer semi-circle boundary far from the crack, displacement boundary conditions were used to impose an asymptotic dependence on the elastic crack tip singular field of Irwin (1960). The diameter of the pre-existing voids was a_o as was the initial COD of the crack. The distance from the center of the void to the center of the crack tip was initially D_o and this was also the center-to-center spacing of the voids. Ratios of 10 and 4.5 were used for D_o/d_o in the calculations.

The problems were solved using the ABAQUS (1984) finite element program. The typical mesh in Fig. 15 has 5,535 nodes with 16,605 degrees of freedom and 740 twenty-noded isoparametric brick elements. The mesh was made larger effectively by using an embedding technique developed by McMeeking (1977a) which makes use of a plane strain crack tip blunting, elastic-plastic solution without voids to provide results which were used for the actual boundary condition in the three-dimensional calculation. Further details on the calculations can be found in Hom and McMeeking (1988b).

Deformed Configurations Figures 16 and 17 show two views of the near tip deformed finite element mesh superimposed on the undeformed mesh at a load level of $J/\sigma_0 a_0 = 3.3$ for a non-hardening material with $D_0/a_0 = 4.5$. Figure 16 is a section cut perpendicular to the crack through the center of the void, while Fig. 17 is a section cut in the plane of the crack. Line A-A identifies the crack front in Fig. 17. These figures show that the ligament between the void and the crack is contracting. As it is pulled towards the crack, the hole changes shape and becomes approximately an oblate spheroid whose major axes are in the plane of the crack.

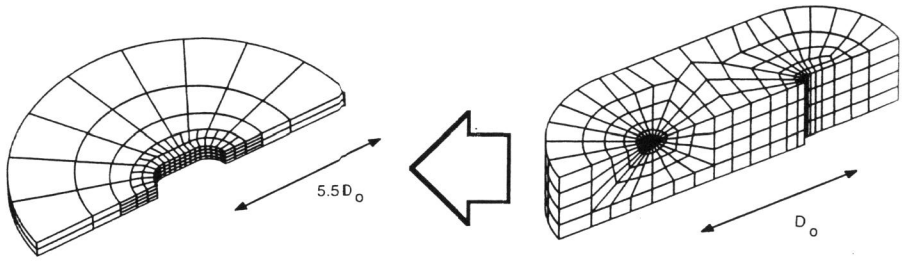

Fig.15. Typical finite element mesh used to solve the problem of three dimensional void growth before a blunting crack tip. The mesh in Figure (a) surrounds the mesh in Figure (b).

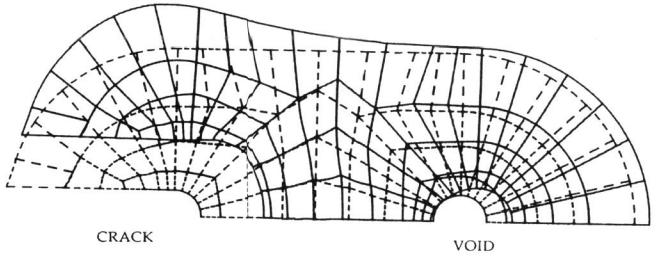

Fig.16. The deformed mesh in the near tip region for a section cut which is perpendicular to the crack and which passes though the center of the void. The material is perfectly plastic and the load level is $J/\sigma_0 a_0 = 3.3$.

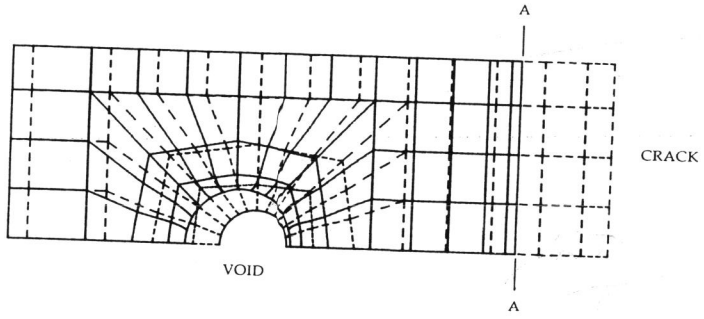

Fig.17. The deformed mesh asfor Fig. 16 but for a section in the crack plane.

Crack Tip Opening and Hole Growth Figure 18 shows the hole growth magnitudes, the crack tip opening displacement (COD) and the ligament size between the void and the crack tip as functions of the applied load for the void spacing $D_0/a_0 = 4.5$ in the perfect plasticity case. The parameter b is the current COD, and D is the current ligament size. The quantities a_1, a_2 and a_3 are the hole's dimensions in the deformed configuration as illustrated in the figure inset. The holes expand in every direction, but the voids grow fastest towards the crack tip and towards neighboring voids and thus become oblate as indicated above. The void's axis a_2 grows at approximately half the rate of the other two axes and the effect is distinct. This shows that the interaction between the void and the crack is strong and overcomes the effect of the mainly tensile stress field ahead of the crack tip which would be expected to elongate the void in the tensile direction. Throughout the load history, a_3 is approximately equal to a_1, indicating that there is also interaction between neighboring voids ahead of the crack tip. However, the ligament between the crack and the voids is still smaller and contracting at a faster rate than the ligament between neighboring voids because of relative motion of the crack tip towards the voids induced by the void-crack interaction. Therefore the voids interact more strongly with the crack than they do with one another. Aravas and McMeeking (1985a) also found that cylindrical voids grow fastest in the direction towards the crack tip. However, their cylindrical voids grew approximately five times the rate of our initially spherical voids. This indicates that void growth strongly depends on the shape of the void with holes which individually extend far along the front of the crack being free to grow rapidly. This effect must be a strong void-crack interaction since it is not suggested by what is known about the growth of isolated cylindrical and spherical voids (McClintock (1968) and Rice and Tracey (1969). The results can be compared with predictions using the model of Rice and Tracey (1969) for an isolated spherical void under a remote uniform loading which is taken as the crack tip field. For the perfect plasticity case, the voids in the finite element calculation grow at twice the rate predicted from the Rice and Tracey model. Also in Rice and Tracey's analysis the void diameter a_2 grows faster than the other void dimensions, contrary to the more accurate finite element calculation. It is interesting to note that the predicted growth of the void's vertical dimension a_2 is roughly the same for the analysis of Rice and Tracey and the finite element calculation. Therefore, vertical growth of the hole seems unaffected by interaction with the crack and neighboring voids.

Near Tip Plastic Strain and Stress Distributions Figure 19 is a contour plot of the effective plastic strain $\bar{\varepsilon}^p$ in the near tip region for the perfect plasticity case with $D_0/a_0 = 4.5$ and $J/\sigma_0 a_0 = 3.3$. There are large plastic strains near the void and in the ligament between the crack and the void. In Fig. 19, a view of the the crack plane, the contour levels when the voids are not present are also plotted with dashed lines. It can be seen that around the voids the level of effective plastic strain has been greatly elevated and this effect spreads sideways between neighboring voids.

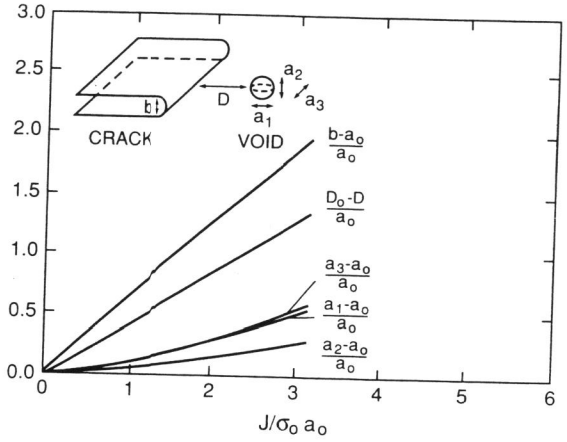

Fig.18. Plot of the COD the ligament between the crack tip and the hole, and the void's dimensions versus applied load for a material with $N = 0$.

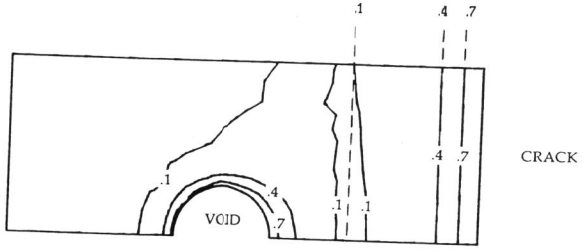

Fig.19. Contour plot of $\bar{\varepsilon}^p$ in the near crack tip region a section in the crack plane. The dashed lines indicate the contour levels when the voids are not present.

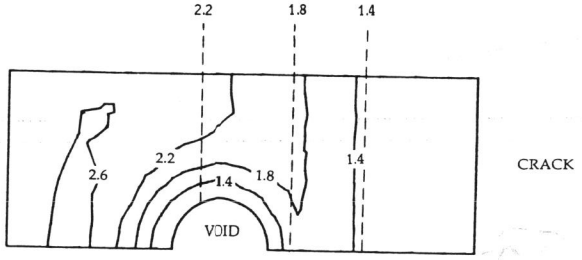

Fig. 20. Contour plot of hydrostatic stress ($\sigma_{kk}/3$) in the near crack tip as for Fig. 19. The dashed lines indicate the contour levels when the voids are not present.

Figure 20 is a contour plot of the hydrostatic stress $\sigma_{kk}/3$ in the near tip region for $D_0/a_0 = 4.5$ and $N = 0$ when $J/\sigma_0 a_0 = 3.3$. In the plan view of Fig. 20, the dashed lines indicate the contour levels when the voids are not present. The void is closer to the crack tip at this stage than the position of the maximum in hydrostatic stress when there is no void. As a consequence the hydrostatic stress in the ligament is relatively low anyway. Comparison of the dashed lines with the full contours indicates a slight drop in the hydrostatic stress in the ligament due to the presence of the voids. Of course, around the void the hydrostatic stress is low because of the free surface. Parallel to the crack front, the triaxiality has built up to nominal levels within about one current void radius. From Fig. 20, we can conclude that the presence of the void does not elevate the hydrostatic stress in the ligament significantly but has a more marked effect on the material between neighboring voids.

Figure 21 shows, for different load levels, the true stress σ_{yy} in the ligament versus r, the distance from the crack tip. The distance has been normalized by the initial void diameter a_0. The arrows on the r/a_0 axis indicate the position of the surface of the hole nearest to the crack. In the ligament, σ_{yy} decreases with increasing load. At the free surfaces of the void and the crack tip the hydrostatic stress is low due to the fact that deviatoric stresses are bounded by the yield condition and the normal tractions are zero. The hydrostatic stress in the ligament builds up away from the free surfaces and due to stress equilibrium the magnitude of the stress is determined by the distance from the void or the crack tip. Since the ligament is getting narrower with increasing load, there is less distance for the build up of hydrostatic stress at higher load levels; therefore the peak value of σ_{yy} decreases with increasing J. Similar results were observed by Aravas and McMeeking (1985a) for cylindrical holes before a blunt crack tip.

The results of the finite element calculation indicate that spherical voids have a much smaller effect on the near crack tip behavior than elongated voids. Spherical voids seem to act as local perturbations to the stress field generated by the crack tip, so the presence of the voids does not drastically affect the crack tip's behavior. Only in the later stages of void growth, when the void is very large compared with the ligament, does the presence of the void influence the crack tip. On the other hand, cylindrical voids have a more substantial effect on the near tip fields. Aravas and McMeeking (1985a) have shown that elongated holes interact with the crack tip at the early stages of loading. This interaction strongly affects the behavior of the crack tip. Indeed at later stages of crack opening, Aravas and McMeeking found that an elongated void directly ahead of the crack and parallel to the tip actually acts as the blunt crack tip.

HOLE COALESCENCE AND FRACTURE INITIATION

In metals, ductile crack advance occurs when individual voids or concentrations of voids coalesce with the crack tip. The process is often initiated when shear localization due to microvoid growth develops in the ligament between the

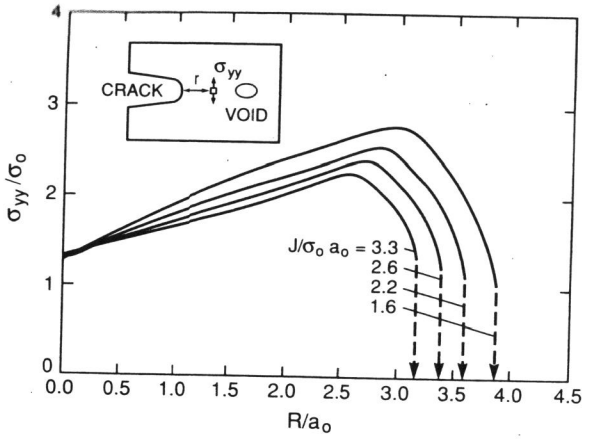

Fig. 21. Plot of the stress σ_{yy}/σ_o along the ligament between the crack tip and the hole at different load levels for a material with $N = 0$.

TABLE I

	N = 0		N = 0.2	
	$D_o/a_o = 4.5$	$D_o/a_o = 10.$	$D_o/a_o = 4.5$	$D_o/a_o = 10.$
$D = 0$	1.49	1.73	2.31	2.35
$a_2 = D$	1.01	1.40	1.43	1.95
$a_1 = .83\ D$	0.83	1.21	1.59	1.84

The ratio b_f/D_o for various void coalescence criteria computed from the finite element results of Hom and McMeeking (1988b)

crack tip and neighboring voids. Several criteria for determining when coalescence involving major voids occurs have been proposed based on the length of the ligament relative to the void's dimensions. Hom and McMeeking (1988b) use three of these criteria to interpret their void growth results and to predict COD values for fracture initiation. Rice and Johnson (1970) proposed that coalescence occurs when the size of the ligament between the crack tip and the void is equal to the vertical dimension of the hole. This criterion is $D = a$. Le Roy, Embury, Edwards and Ashby (1981) formulated a similar criterion based on experimental observation of spheroidized carbon-steels under tensile strain. They proposed that void linkage occurs when the longest axis of the void is of the order of magnitude of the mean planer nearest neighbor spacing, or $a^{max} = \phi D$. The parameter ϕ is an experimentally determined constant, which is 0.83 for voids nucleated from spherical particles and 1.23 for voids nucleated from elongated particles. From the computations of Hom and McMeeking (1988b), a_1 is the largest dimension of the initially spherical void, so the criterion for this model becomes $a_1 = 0.83\ D$. Finally, a conservative upper bound to coalescence is the criterion that the ligament must neck down to a point. This means $D = 0$.

Estimates for the notch width at fracture initiation b_f have been obtained by Hom and McMeeking (1988b) using the finite element calculations and the three coalescence criteria just discussed. Fracture initiation was identified with the coalescence of the voids separately with the crack tip. The finite element calculations were terminated well before these processes of coalescence would have commenced. However using the rates of void growth, crack tip blunting and ligament contraction prevailing when the numerical analysis was stopped, Hom and McMeeking (1988b) were able to extrapolate the results to obtain values for the near tip dimensions at the time of coalescence. Table I shows the predictions for b_f in the four cases examined. The results are very dependent on inclusion spacing and void size. In contrast, Aravas and McMeeking (1985a) found that for cylindrical voids b_f/D is nearly independent of D/a. Therefore, b_f is more sensitive to the size of the spherical inclusions than it is to the inplane dimensions of long cylindrical inclusions when they are controlling ductile fracture initiation.

The COD at fracture initiation has been measured by several researchers experimentally, and Fig. 22 is a summary of those results plotted in the form of b_f versus inclusion spacing. Most of the experimental results are for approximately spherical inclusions loosely bonded to the matrix. The predictions of the finite element calculations of Hom and McMeeking (1988b) have been plotted with the criterion $D = a$ and they agree quite well with the experimental data. The results of the models of Rice and Johnson (1970) and McMeeking (1977a) have been plotted also for comparison with the finite element results. Their results tend to overestimate the COD at fracture initiation. The finite element results of Hom and McMeeking (1988b) predict an earlier coalescence due to a strong void-crack interaction influencing the void growth. Also plotted in Fig. 22 are the results of Aravas and McMeeking (1985a).

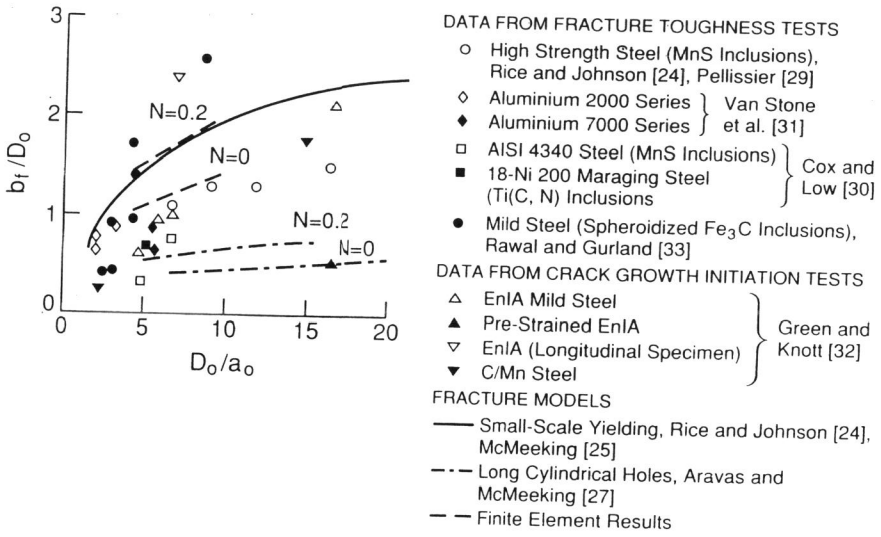

Fig. 22. Experimental data and finite element predictions for the COD at initiation of crack growth or fracture, related to particle spacing D_o and particle size a_o. Also plotted are results for fracture due to elongated voids from a model by Aravas and McMeeking (1985a), and due to spherical voids from models by Rice and Johnson (1970), and McMeeking (1977a).

As expected their cylindrical voids coalesce before the initially spherical voids and lead to a lower fracture toughness for crack growth initiation.

CLOSURE

Substantial progress has been made in the numerical analysis of crack blunting and near tip void growth. In addition, the results are in reasonable agreement with experiments measuring surface deflections and the initiation of ductile crack propagation. Substantial work remains to be done on void nucleation and coalescence including the effects of shear banding. Such work should clarify the distinctions and discrepancies between experimental data and numerical results which remain in the ductile crack propagation area.

ACKNOWLEDGEMENTS

The research reviewed here has been supported by a series of National Science Foundation Grants from the Solid Mechanics Program. The provision of the ABAQUS program by Hibbitt, Karlsson and Sorensen, Inc. of Providence, Rhode Island, is gratefully acknowledged.

REFERENCES

ABAQUS, (1984), User's Manual, Version 4.5, Hibbitt, Karlsson and Sorensen, Inc., Providence, RI 02906.

Achenbach, J. D. and V. Dunayevsky, (1984), *J. Mech. Phys. Solids*, 32, 89.

Andersson, H., (1977), *J. Mech. Phys. Solids* 25, 217.

Aoki, S., Kishimoto, K., Takeya, A. and Sakata, M., 1984, *Int. J. Fracture*, 24, 267.

Aravas, N. and R. M. McMeeking, (1985a), *J. Mech. Phys. Solids*, 33, 25.

Aravas, N. and R. M. McMeeking, (1985b), *Int. J. Fracture*, 29, 21.

Argon, A. S. and J. Im, (1975), *Metall Trans.*, 6A, 839.

Brown, L. M. and J. D. Embury, (1973), *Proc. 3rd Int. Conf. Strength of Metals and Alloys*, Cambridge, U. K., p.164.

Chiang, W. T., (1981), *Advances in Fracture Research*, Proc. 5th Int. Cong. Fracture (ICF5) (edited by D. Francois) Vol. 1, p. 235, Pergamon.

Christoffersen, J. and J. W. Hutchinson, (1979), *J. Mech. Phys. Solids*, 27, 465.

Clayton, J. Q. and J. F. Knott, (1976), *Metal Sci.* ,10, 63.

Cox, T. B. and J. R. Low, (1974), *Metall. Trans.* 5, 1457.

Dugdale, D. S., (1960), *J. Mech. Phys. Solids*, 8, 100.

Green, G., and J. F. Knott, (1976), *J. Eng. Mater. Tech* 98, 37.

Gurson, A. L., (1977a), *Trans. ASME* 99, Series H, *J. Eng. Matl. Tech.* 37.

Gurson, A. L., (1977b), *Fracture 1977, Proc. 4th Int. Conf. Fracture* (ICF4) (edited by D. M. R. Taplin) 2, p. 357. Pergamon Press, Oxford.

Hom, C. L. and R. M. McMeeking, (1988a), "Large Crack Tip Opening in Elastic-Plastic Sheets", to appear in *Int. J. Fracture.*

Hom, C. L. and R. M. McMeeking, (1988b), "Three-Dimensional Void Growth Before a Blunting Crack Tip", to appear in *J. Mech. Phys. Solids.*

Hutchinson, J. W., 1968a, *J. Mech. Phys. Solids*, 16, 13.
Hutchinson, J. W., (1968b), *J. Mech. Phys. Solids*, 16, 337.
Irwin, G. R., (1960), *Structural Mechanics* (Proceedings of First Symposium on Naval Structural Mechanics, Stanford, 1959) (edited by J. N. Goodier and N. J. Hoff), p. 557. Pergamon Press, Oxford.
Le Roy, G., J. D. Embury, G. Edward, and M. F. Ashby, (1981), *Acta Metall.*, 29, 1509.
McClintock, F. A., (1968), *J. Appl. Mech.*, 35, 363.
McClintock, F. A., (1971), *Fracture: An Advanced Treatise* (edited by H. Leibowitz) Vol 3, p. 47, Academic Press.
McMeeking, R. M., (1977a), *J. Mech. Phys. Solids*, 25, 371.
McMeeking, R. M., (1977b), *J. Eng. Mater. Tech*, 99, 290.
McMeeking, R. M. and D. M. Parks, (1979), *Elastic-Plastic Fracture*, ASTM STP 668, p. 175, ASTM.
McMeeking, R. M. and J. R. Rice, (1975), *Int. J. Solids Struct.*, 11, 601.
Nagtegaal, J. C., D. M. Parks,. and J. R. Rice, (1974), *Comp. Methods Appl. Mech. Eng.*, 4, 153.
Nakamura, T. and D. M. Parks, (1987), "Three-Dimensional Stress Field Near the Crack Front of a Thin Elastic Plate," Mechanic of Material Report, MIT.
Narasimhan, R. and A. J. Rosakis, , (1988), *J. Mech. Phys. Solids*, 36, 77.
Needleman, A. and V. Tvergaard, D. M., (1983), *Elastic-Plastic Fracture* ASTM STP 803, p. 80. ASTM.
Nishimura, N. and J. D. Achenbach., (1986), *J. Mech. Phys. Solids*, 34, 147.
Pellissier, G.E., (1968), *Eng. Fracture Mech.*, 1, 55.
Rawal, S. P. and J. Gurland, (1976), *Proc. 2nd Conf. Mechanical Behavior of Materials* (Boston, 1976), p. 1154. Federation of Materials Societies, Dearborn, Michigan.
Rice, J. R., (1968), *J. Appl. Mech.*, 35, 379.
Rice, J. R., (1976), The Mechanics of Fracture (edited by F. Erdogan) ASME AMD-19, p. 23, ASME.
Rice, J. R. and M. A. Johnson, (1970), *Inelastic Behavior of Solids* (edited by M. F. Kanninen, , W. F. Adler, A. R. Rosenfield and R. I. Jaffe), p. 641. McGraw-Hill, New York.
Rice, J. R. and G. F. Rosengren, (1968), *J. Mech. Phys. Solids*, 16, 1.
Rice, J. R. and D. M. Tracey, (1969), *J. Mech. Phys. Solids*, 17, 201.
Rodgers, H. C., (1960), *Trans. Metall. Soc. AIME* 218, 498.
Rudnicki, J. W. and J. R. Rice, (1975), *J. Mech. Phys. Solids*, 23, 371.
Thomason, P. F., (1979), *Fracture Mechanics in Engineering Application* (edited by G. C. Sih and S. R. Valluri) p. 43, Sijthoff and Noordhoff.
Tvergaard, V., (1982), *Int. J. Solids Structures*, 18, 659.
Tvergaard, V. and A. Needleman, 1984, Acta Metall., 32, 15.
Van Stone, R.H., R.H. Merchant, and J. R. Low (1974), *Fatigue and Fracture Toughness-Cryogenic Behavior*, ASTM STP 556, p. 93, ASTM.
Wu, X. P. and F. P. Chiang, (1986), "Three-Dimensional Crack-Tip Deformation in a Plastically Deformed Three-Point Bend Specimen," Technical Report No. 475, SUNY-Stony Brook.